AIP Journal of Applied Physics

Soft mobile robots driven by foldable dielectric elastomer actuators

Wenjie Sun, Fan Liu, Ziqi Ma, Chenghai Li, and Jinxiong Zhou

Citation: Journal of Applied Physics **120**, 084901 (2016); doi: 10.1063/1.4960718
View online: http://dx.doi.org/10.1063/1.4960718
View Table of Contents: http://scitation.aip.org/content/aip/journal/jap/120/8?ver=pdfcov
Published by the AIP Publishing

Soft mobile robots driven by foldable dielectric elastomer actuators

Wenjie Sun, Fan Liu, Ziqi Ma, Chenghai Li, and Jinxiong Zhou[a)]
State Key Laboratory for Strength and Vibration of Mechanical Structures and School of Aerospace, Xi'an Jiaotong University, Xi'an 710049, China

(Received 21 June 2016; accepted 29 July 2016; published online 22 August 2016)

A cantilever beam with elastic hinge pulled antagonistically by two dielectric elastomer (DE) membranes in tension forms a foldable actuator if one DE membrane is subject to a voltage and releases part of tension. Simply placing parallel rigid bars on the prestressed DE membranes results in enhanced actuators working in a pure shear state. We report design, analysis, fabrication, and experiment of soft mobile robots that are moved by such foldable DE actuators. We describe systematic measurement of the foldable actuators and perform theoretical analysis of such actuators based on minimization of total energy, and a good agreement is achieved between model prediction and measurement. We develop two versions of prototypes of soft mobile robots driven either by two sets of DE membranes or one DE membrane and elastic springs. We demonstrate locomotion of these soft mobile robots and highlight several key design parameters that influence locomotion of the robots. A 45 g soft robot driven by a cyclic triangle voltage with amplitude 7.4 kV demonstrates maximal stroke 160 mm or maximal rolling velocity 42 mm/s. The underlying mechanics and physics of foldable DE actuators can be leveraged to develop other soft machines for various applications. *Published by AIP Publishing*. [http://dx.doi.org/10.1063/1.4960718]

I. INTRODUCTION

Folding—an operation of deforming, mostly uncut thin sheets, into decorative or well-defined shapes through bending without stretching and tearing—has evolved from an ancient art for aesthetic purpose to a modern technology for functional materials and structures.[1–5] The concept of folding can span from molecular length scale DNA folding to very large scale deployable aerospace structures such as solar sails and panels.[4–7] Folding, in particular, origami-inspired self-folding, has also grown into a manufacturing technology to fabricate multifunctional materials, transforming architectures, robots, and self-folding machines.[4–12] Advantages of using folding technology to fabricate, assembly, and morph materials and structures include compact storage of extendable structures, invasive manipulation and control at very small or very large scales or in remote applications, and reduction of manufacture complexity, etc.

One popular way to realize folding is to leverage active materials, which can deform and morph in response to a variety of external stimuli. Typical active materials for folding include shape memory alloys (SMA),[4] shape memory polymers (SMP),[11] polymer gels,[12–15] temperature or light-sensitive polymers,[16,17] and dielectric elastomers (DE).[18–20] More recently, there has been an upsurge of interests to develop folding structures by using soft active materials as listed above, since soft materials are easy to fold or unfold elastically, sensitive to diverse stimuli, inexpensive and easy to integrate with other inactive materials. Among these soft active materials, DE is a potential candidate for folding applications since it has fast response speed (3 s for silicone elastomer DC3481), large actuation deformation (hundreds or even one thousand strain), high electromechanical efficiency (theoretically 90%), highenergy density (560 J/kg for equi-biaxial loading), and negligible hysteresis if silicone elastomer is used.[21–25]

Foldable deformations or motions can be driven by soft DE in various proposed configurations which mainly work in an antagonistic manner.[18,26–28] Folding of these soft devices is driven by antagonistic and agonistic components often occur in pair. As one component contracts or expands, the other relaxes or contracts. Lochmatter and Kovacs[26] presented design and characterization of an active hinge segment performing rotary motions back and forth. Wingert *et al.*[27] designed a bistable DE actuator driven by antagonistic mechanism and demonstrated a 6 degree-of-freedom binary manipulator. Similar bistable antagonistic DE actuators were presented by Chouinard and Plante for binary robots.[28] Recently, Shintake *et al.*[18] reported a foldable antagonistic DE actuator with elastic hinges to drive the folding of the elevon of a 130 g micro-air vehicle (MAV). Comparing with other foldable antagonistic DE actuators, use of elastic hinges enables foldability with simple structures.

Since folding or bending is a basic deformation mode essential for the development of robots, the foldable antagonistic scheme can be exploited for other robots development. Here, we describe the design, analysis, fabrication, and demonstration of a soft mobile robot driven by enhanced foldable DE actuators. Different from the Shintake's design of foldable actuator, where only one patch of a DE membrane is working in a pure shear deformation,[18] we introduce unidirectional constraint and achieve a DE membrane with multiple active regions all work in a pure shear deformation, an effective strategy which is well-understood and validated previously both theoretically and experimentally.[29–31] The enhanced foldable DE actuator in combination with ratchet-wheels results in a soft mobile rolling robots. We investigate

[a)]Author to whom correspondence should be addressed. Electronic mail: jxzhouxx@mail.xjtu.edu.cn

several design parameters and finally demonstrate the locomotion of the soft robot.

II. FOLDABLE DIELECTRIC ELASTOMER ACTUATORS

Fig. 1(a) presents the CAD design and key components of a pair of foldable DE actuators, which consist of four prestretched DE membranes connected via a rigid spacer (Poly(methyl methacrylate) (PMMA)) and an elastic cantilevered hinge (Polyimide (PI)). The hinge is placed symmetrically across the spacer and the top and bottom DE membranes, making the top and bottom DE membranes work in an antagonistic manner. Two parallel PMMA bars are placed on each DE membrane to maintain the prestretch in the direction parallel with bars (marked as 1) and bring DE membrane with three active regions in series and all work in a pure shear state (along direction 2 marked in the figure). Due to symmetry, Fig. 1(b) schematizes the front view of one foldable DE actuator used for experimental measurement. Keeping the prestretch in direction 1 fixed while tuning the unbalanced prestretch in direction 2, the system takes a reference state (left) with an initial folding angle θ_0. When a voltage is applied to the top DE, the internal stress in the top DE is released and the actuator bends downward and achieves the final actuated state (right)

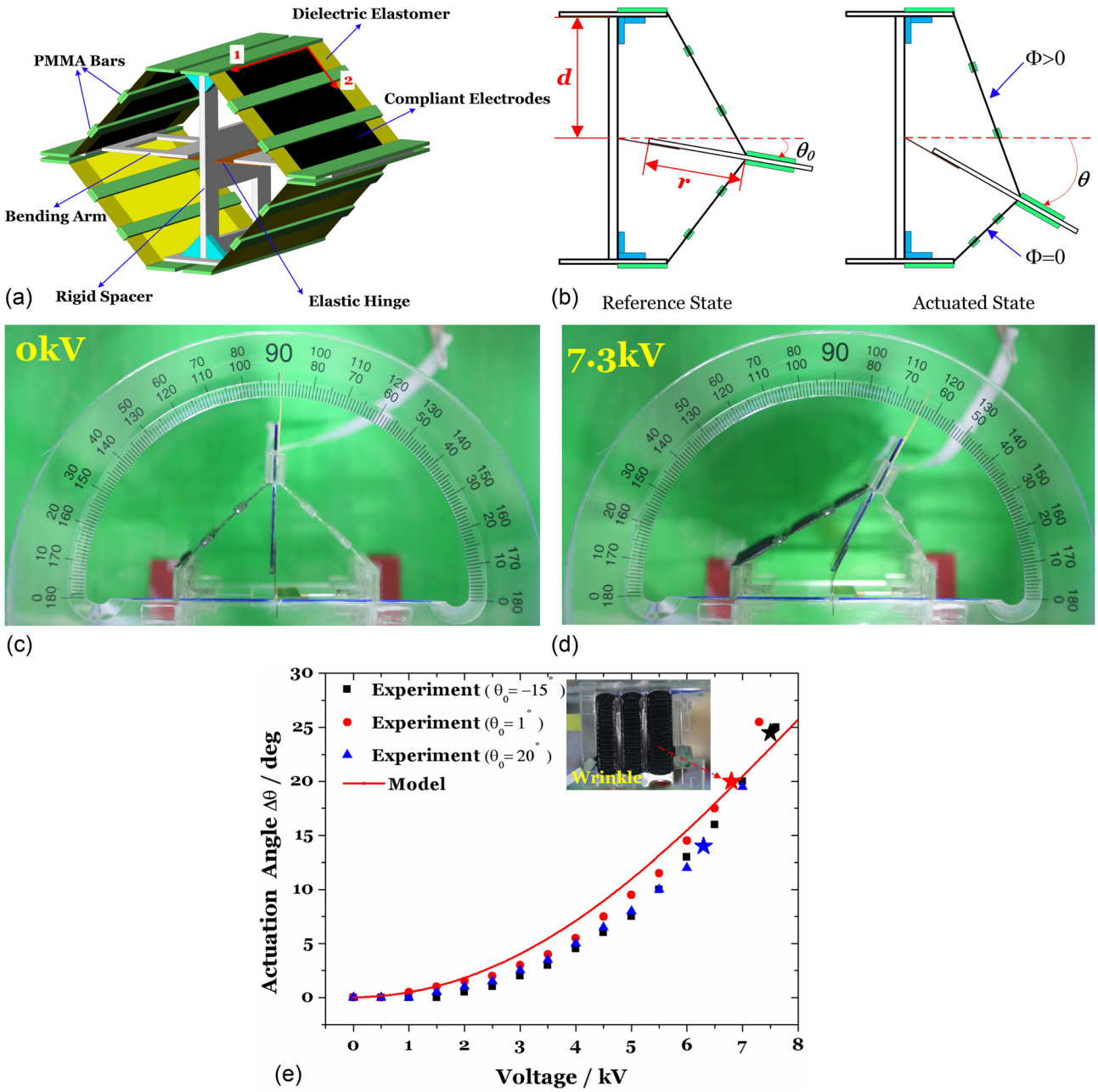

FIG. 1. CAD design, schematic, experimental measurement and model prediction of an enhanced foldable DEA. (a) CAD design of a pair of enhanced foldable DE actuators connected via a rigid spacer and an elastic hinge. Two parallel bars are placed on a pre-stretched DE membrane to maintain prestretch in direction 1 to enhance electromechanical performance of DE. (b) Front view and working mechanism of the enhanced foldable DE actuator. (c) Measurement of folding angle for reference (left) and actuated state (right) at applied voltage 7.3 kV. (d) Actuation angles $\Delta\theta = \theta - \theta_0$ versus applied voltage for three initial folding angles (markers) together with the result of model prediction by minimization of total energy of the system with respect to the actuation angle.

with current folding angle θ, defining actuation angle as $\Delta\theta = \theta - \theta_0$. Fig. 1(c) shows experimental measurement of a folding angle for reference (left) and actuated state (right) at applied voltage 7.3 kV.

To better understand the behavior of the foldable antagonistic DE actuator, we present a model prediction of the actuator based on minimization of total energy of the system.[18–20] Concerning the foldable DE actuator shown in Figs. 1(b) and 1(c), the system has three deformable elements: top active DE membrane, bottom passive membrane, and the elastic hinge. The top DE membrane has both elastic energy due to stretching of polymers and electrostatic energy due to polarization, $W_{ela}^{Top} + W_{ele}^{Top}$; only elastic energy, W_{ela}^{Bottom}, is stored in the bottom membrane; the elastic hinge takes strain energy, W_{ela}^{Hinge}, due to bending of the hinge. Suppose a piece of incompressible DE membrane with reference dimensions $W_0 \times L_0 \times H_0$ in three directions 1, 2, and 3 is deformed to $\lambda_1 W_0 \times \lambda_2 L_0 \times H_0/(\lambda_1\lambda_2)$ under combined mechanical and electrical loadings. The stretch in direction 1 is fixed to be $\lambda_1 = \lambda_1^p$ after mechanical prestretch and is the same for both top and bottom membranes. The stretch in direction 2 is a function of actuation angle $\Delta\theta$ and different for top and bottom membranes, calculated as $\lambda_2^{Top}(\Delta\theta) = \frac{\sqrt{r^2+d^2+2rd\sin(\Delta\theta)}}{L_0}$ and $\lambda_2^{Bottom}(\Delta\theta) = \frac{\sqrt{r^2+d^2-2rd\sin(\Delta\theta)}}{L_0}$, respectively, with r being length of the bending arm, and d is half of the height of spacer shown in Fig. 1(b). Adopting the Neo-Hookean model to describe energy due to stretching of polymer network, the elastic energy per unit reference volume is given as $\frac{\mu}{2}\left(\lambda_1^2 + \lambda_2^2 + \lambda_1^{-2}\lambda_2^{-2} - 3\right)$ with μ being shear modulus of the membrane. We assume the top DE membrane follows the widely used ideal dielectric model,[32] the energy due to polarization per unit volume is thus $\frac{1}{2}\varepsilon E^2$ with ε being permittivity of the DE membrane and $E = \frac{V}{H_0}\lambda_1\lambda_2$ being the electrical field in a deformed state. The free energy of the top DE membrane is thus written as a function of actuation angle $\Delta\theta$ as

$$W^{Top}(\Delta\theta) = W_0 L_0 H_0 \frac{\mu}{2}\left(\lambda_1^2 + (\lambda_2^{Top}(\Delta\theta))^2 + \lambda_1^{-2}(\lambda_2^{Top}(\Delta\theta))^{-2} - 3\right) + \frac{\varepsilon V^2}{2H_0} W_0 L_0 \lambda_1^2 (\lambda_2^{Top}(\Delta\theta))^2, \quad (1)$$

where V is the applied voltage to the top membrane. The elastic energy of the bottom membrane only takes the first term in Eq. (1) and is expressed as $W^{Bottom}(\Delta\theta) = W_0 L_0 H_0 \frac{\mu}{2}(\lambda_1^2 + (\lambda_2^{Bottom}(\Delta\theta))^2 + \lambda_1^{-2}(\lambda_2^{Bottom}(\Delta\theta))^{-2} - 3)$. Approximating the elastic hinge as an elastic spring, its strain energy is $W_{ela}^{Hinge}(\Delta\theta) = \frac{1}{2}k(\Delta\theta)^2$ with stiffness evaluated as $k = \frac{E_h w_h h_h^3}{12 l_h}$. At given applied voltage, the total energy of the foldable actuator is a nonlinear function of $\Delta\theta$, i.e.,

$$W_{total}(\Delta\theta) = W^{Top}(\Delta\theta) + W^{Bottom}(\Delta\theta) + W_{ela}^{Hinge}(\Delta\theta). \quad (2)$$

The system equilibrates under the condition that the total energy of the system minimizes with respect to $\Delta\theta$, i.e.,

$$\frac{dW_{total}(\Delta\theta)}{d(\Delta\theta)} = 0. \quad (3)$$

Fig. 1(d) presents the measurement of actuation angles versus applied voltage for three initial folding angles (markers) in together with the model prediction result (red solid line). Parameters for model analysis of our foldable actuator are: $W_0 = 23.3$ mm, $L_0 = 34$ mm, $H_0 = 1$ mm, $\mu = 60$ kPa, $r = 30$ mm, $d = 30$ mm, the modulus of the hinge $E_h = 500$ MPa, hinge width $w_h = 30$ mm, hinge thickness $h_h = 0.3$ mm, hinge length $l_h = 6$ mm, and $\lambda_1^p = 3$ fixed during our experiment. Concerning the actuation angles, experimental results for three initial folding angles vary nearly the same and correlate well with the model prediction. Also note that upon a high applied voltage close to 7 kV, wrinkles (inserted image in (c)) along direction 1 were observed with critical voltage marked by stars.

III. SOFT ROBOTS DRIVEN BY FOLDABLE ACTUATORS

Fig. 2 gives the pictures of two types of soft mobile robots driven by foldable DE actuators. The soft robot is composed of two pairs of rigid wheels, two foldable DE actuators, and two cantilever PMMA struts connecting the DE actuators and the axles of wheels. Foldable DE actuators have top active membranes and bottom passive membranes, and the bottom passive membranes can be replaced by elastic springs, giving two prototypes shown in Figs. 2(a) and 2(b), respectively. Two gears are installed coaxially with the wheels, and two patches of glass fiber (thickness 0.25 mm) mounted on the struts work as pawls that engage the teeth of gears, enabling unidirectional locomotion of the soft robot.

We investigate systematically several issues related to locomotive capability of the soft mobile robots. The DE membrane we used in our experiment is the acrylate elastomer, VHB 4910 (3 M company). For the mobile robots installed with DE actuators made of viscoelastic materials, voltage ramping rate would affect the stroke as well as the rolling velocity of the soft robot, and should be the key issue probed first. Fig. 3(a) plots the cyclic triangle voltage with amplitude voltage fixed to be 7.4 kV, and the period of the triangle voltage, T varied from 2 s to 40 s. The applied voltage is ramped from 0 to 7.4 kV in one quarter of the period. Figs. 3(b) and 3(c) plot the measured stroke and rolling velocity versus voltage ramping rate for robots with top and bottom DE membranes and top DE membranes and bottom elastic springs, respectively. Figs. 3(b) and 3(c) reveal that the higher the ramping rate and the higher the rolling velocity of the robot, but the smaller the stroke within one cycle. This is easy to be understood by noting that the VHB elastomer used in our experiment is a highly viscoelastic material with characteristic relaxation

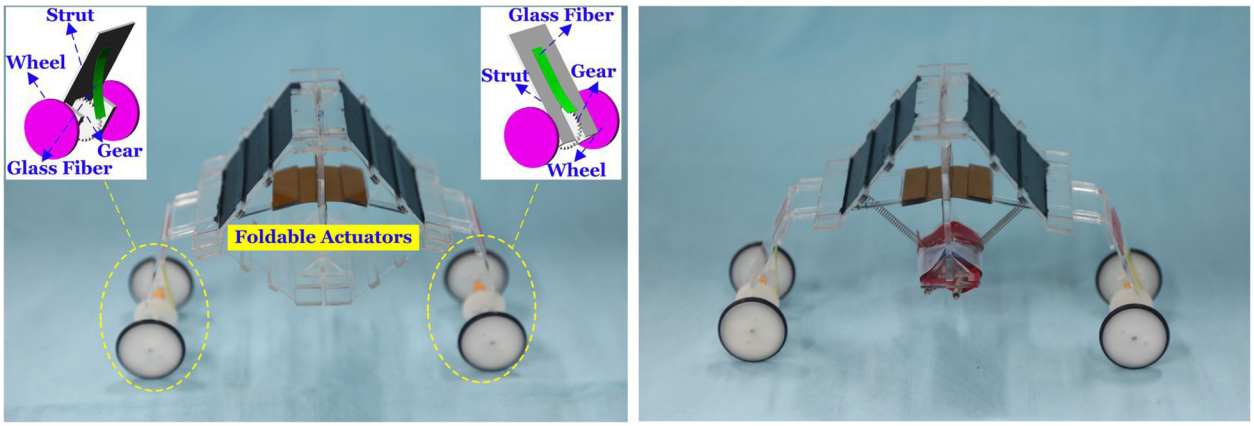

FIG. 2. Two types of assembled soft mobile robots driven by foldable DE actuators. The foldable deformation of the DE actuator in combination with ratchet-wheels results in unidirectional locomotion of the robots. (a) Soft robot has two top active DE membranes and two bottom passive membranes. (b) Replacing two bottom passive membranes by elastic springs results in another version of the soft robot.

time approximately hundreds of seconds,[33] which is much larger than one quarter of the period of the cyclic triangle voltage, 0.05 s–10 s, used in our experiment to ramp up voltage from zero to peak value or ramp down from peak to zero. At higher voltage ramping rate, the DE responses quickly and the robot exhibits higher rolling velocity, but, due to viscoelasticity, the DE membrane does not have enough time to relax to its fully deformed state thus exhibits smaller stroke. Also note that replacing passive DE membranes by suitably selected elastic springs brings

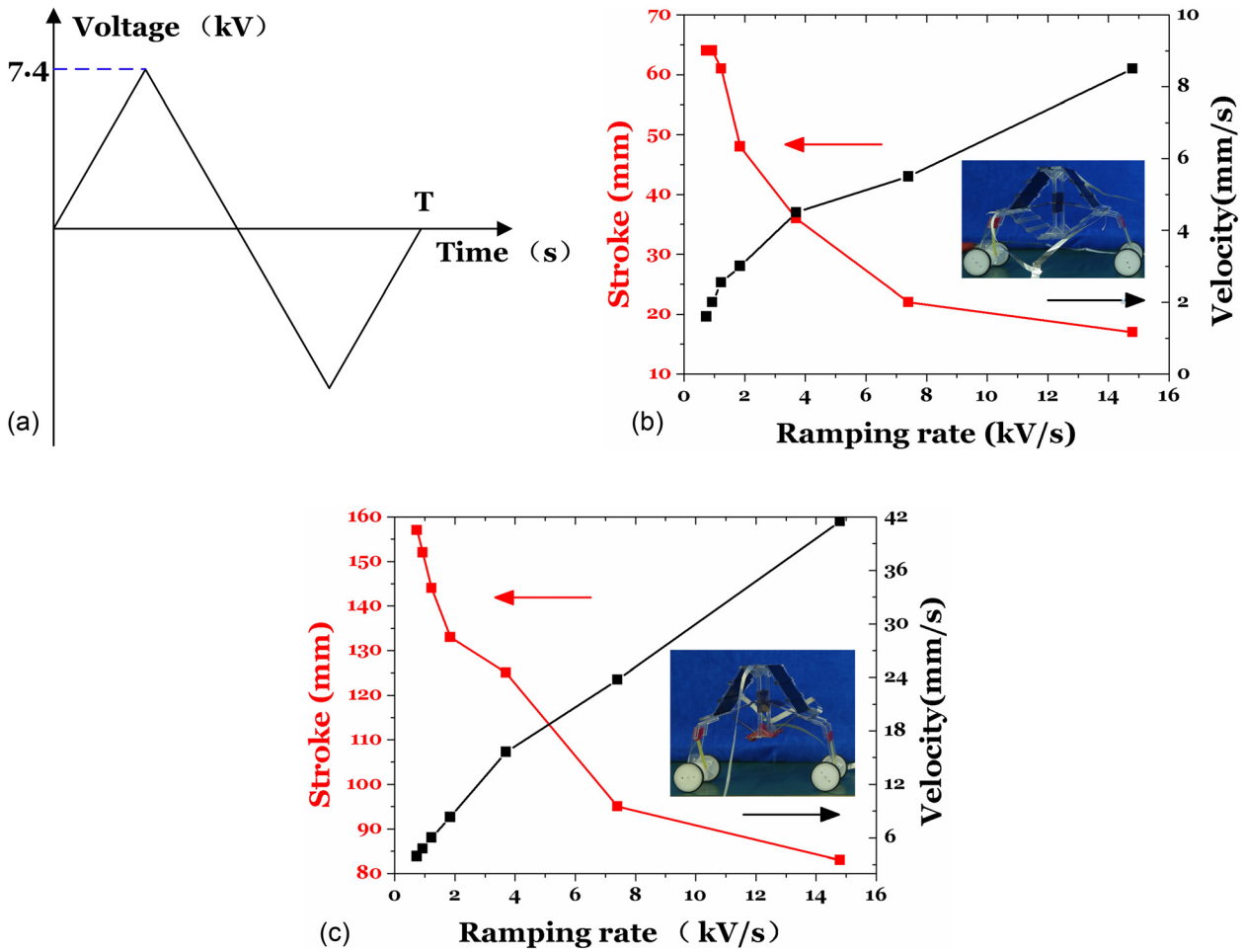

FIG. 3. Locomotive performance of the soft mobile robots for various voltage ramping rates. (a) Applied cyclic triangle voltage with amplitude voltage fixed to be 7.4 kV but various periods to complete one cycle. (b) Stroke and rolling velocity of robots driven by foldable antagonistic actuators by top and bottom DE membranes. (c) Stroke and rolling velocity of robots driven by foldable antagonistic actuators by top DE membrane and bottom elastic springs.

about improvement of locomotive performance of the soft robots-increase of maximal stroke and maximal rolling velocity, i.e., maximal stroke and maximal rolling velocity from 8 mm and 70 mm/s in Fig. 3(b) to 40 mm and 160 mm/s in Fig. 3(c), respectively.

We further probe several key design parameters, e.g., the angle made by the bending arm with the nose or tail strut marked by β in the schematic of Fig. 4(a), and the initial folding angle of the bending arm with respect to the horizontal dashed line denoted by θ_0 in Fig. 4(b). It should be pointed that these two angles are defined as the soft robot fabricated. When the robot is put on the ground, these two angles defined above vary slightly due to gravity of the foldable actuator. For example, if the bending arm of the robot is bent slightly downward as fabricated such that the robot has positive initial folding angle, e.g., $\theta_0 = 10°$, the soft robot morphs a little bit due to gravity and the bending arm keeps nearly horizontal position. Fig. 4 implies that positive initial folding angle as well as nearly perpendicular angle made between bending arm and strut would achieve optimal maximal stroke of the robot. We finally demonstrate the locomotion of the soft mobile robot in Fig. 5, where a series of still frames from experimental video are recorded. A 45 g soft robot driven by a cyclic triangle voltage with amplitude 7.4 kV demonstrates maximal stroke 160 mm ($T = 40$ s, ramping rate = 0.74 kV/s) or maximal rolling velocity 42 mm/s ($T = 2$ s, ramping rate 15 kV/s).

IV. CONCLUSION

In summary, we develop soft mobile robots driven by enhanced foldable dielectric elastomer actuators. Enhancement of foldable actuators is realized by introducing several reinforced rigid bars to maintain prestretch in one particular direction and rendering the actuators work in a pure shear state. We perform measurement and model analysis of the foldable actuators, and a good agreement is achieved. We describe the design, analysis, fabrication, and measurement of the soft robots, and demonstrate the locomotion of the robots. We highlight several key design parameters that affect the locomotion of soft robots. Replacing the antagonistic elastomers by elastic springs results in increased maximal stroke and rolling velocity of the soft robots. The underlying mechanics and physics of the foldable antagonistic dielectric elastomer actuators can be leveraged to develop soft machines for other applications.

We further envision that using dielectric elastomers with negligible viscoelasticity, such as silicone rubbers or natural rubbers, to replace currently used VHB tapes, would demonstrate faster response and resolve the issue of rate-dependence of current prototype of soft robots. In addition, the four wheels of current soft robots are actuated simultaneously with the same forward or backward displacements, rendering locomotion of soft robots only in a straight line. Further development of the soft robots that can exhibit maneuvering is highly desirable, which can be

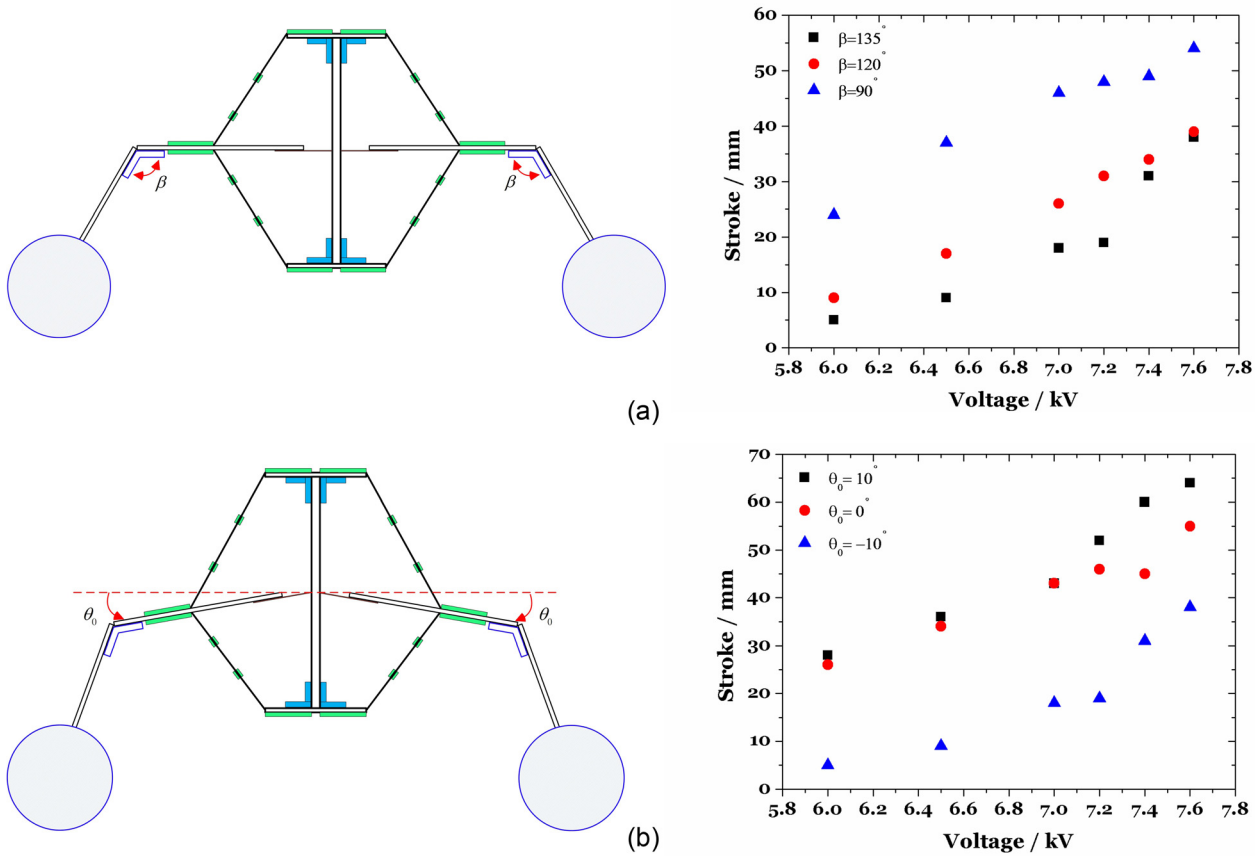

FIG. 4. Effects of two designing angles on the locomotive stroke of the soft robot within one complete cycle. (a) Measured stroke in one complete cycle versus applied voltage for various β, with β defined as the angle made by the bending arm of the DE actuator with either of the nose or tail struts. (b) Influence of initial folding angle θ_0 on the stroke of soft robot. Positive initial folding angle means that the bending arm of a foldable DE actuator is bent clockwise and vice versa.

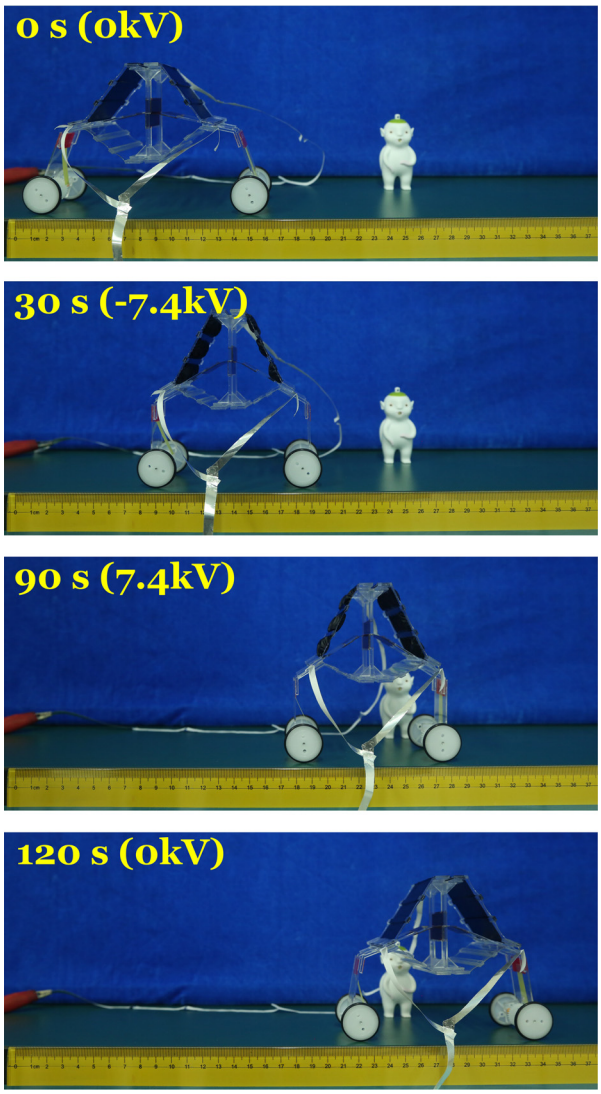

FIG. 5. A series of still frames from experimental video show the self-rolling distance of the soft mobile robot driven by a foldable DE actuator in 120 s (3 periods).

realized by adopting control strategy and driving the wheels separately or introducing the dielectric elastomers enabled soft motors.[34]

ACKNOWLEDGMENTS

This research was supported by the Natural Science Foundation of China (Grant Nos. 11372239, 11472210, and 11321062).

[1]D. Han, S. Pal, J. Nangreave, Z. Deng, Y. Liu, and H. Yan, Science **332**, 342 (2011).
[2]C. Py, P. Reverdy, L. Doppler, J. Bico, B. Roman, and C. N. Baroud, Phys. Rev. Lett. **98**, 156103 (2007).
[3]M. K. Blees, A. W. Barnard, P. A. Rose, S. P. Roberts, K. L. McGill, P. Y. Huang, A. R. Ruyack, J. W. Kevek, B. Kobrin, D. A. Muller, and P. L. McEuen, Nature **524**, 204 (2015).
[4]E. Hawkes, B. An, N. Benbernou, H. Tanaka, S. Kim, E. Demaine, D. Rus, and R. Wood, Proc. Natl. Acad. Sci. **107**, 12441 (2010).
[5]J. L. Silverberg, A. A. Evans, L. McLeod, R. C. Hayward, T. Hull, C. D. Santangelo, and I. Cohen, Science **345**, 647 (2014).
[6]E. A. Peraza-Hernandez, D. J. Hartl, R. J. Malak, Jr., and D. C. Lagoudas, Smart Mater. Struct. **23**, 094001 (2014).
[7]P. M. Liyanage and H. M. Y. C. Mallikarachchi, in Proceedings of the 4th International Conference on Structural Engineering and Construction Management (2013).
[8]D. Rus and M. T. Tolley, Nature **521**, 467 (2015).
[9]Z. Song, T. Ma, R. Tang, Q. Cheng, X. Wang, D. Krishnaraju, R. Panat, C. K. Chan, H. Yu, and H. Jiang, Nat. Commun. **5**, 3140 (2014).
[10]P. M. Reis, F. L. Jiménez, and J. Marthelot, Proc. Natl. Acad. Sci. **112**, 12234 (2015).
[11]S. Felton, M. Tolley, E. Demaine, D. Rus, and R. Wood, Science **345**, 644 (2014).
[12]W. J. Zheng, N. An, J. H. Yang, J. Zhou, and Y. M. Chen, ACS Appl. Mater. Interfaces **7**, 1758 (2015).
[13]J. H. Na, A. A. Evans, J. Bae, M. C. Chiappelli, C. D. Santangelo, R. J. Lang, T. C. Hull, and R. C. Hayward, Adv. Mater. **27**, 79 (2015).
[14]W. guo, M. Li, and J. Zhou, Smart Mater. Struct. **22**, 115028 (2013).
[15]J. L. Silverberg, J. H. Na, A. A. Evans, B. Liu, T. C. Hull, C. D. Santangelo, R. J. Lang, R. C. Hayward, and I. Cohen, Nat. Mater. **14**, 389 (2015).
[16]G. Stoychev, S. Turcaud, J. W. Dunlop, and L. Ionov, Adv. Funct. Mater. **23**, 2295 (2013).
[17]L. Ionov, Soft Matter **7**, 6786 (2011).
[18]J. Shintake, S. Rosset, B. E. Schubert, D. Floreano, and H. R. Shea, IEEE/ASME Trans. Mechatronics **20**, 1997 (2015).
[19]G. Kofod, W. Wirges, M. Paaianen, and S. Bauer, Appl. Phys. Lett. **90**, 081916 (2007).
[20]S. Rosset, O. A. Araromi, J. Shintake, and H. R. Shea, Smart Mater. Struct. **23**, 085021 (2014).
[21]R. Pelrine, R. Kornbluh, Q. Pei, and J. Joseph, Science **287**, 836 (2000).
[22]F. Carpi, S. Bauer, and D. De. Rossi, Science **330**, 1759 (2010).
[23]P. Brochu and Q. B. Pei, Macromol. Rapid Commun. **31**, 10 (2010).
[24]I. A. Anderson, T. A. Gisby, T. G. Mckay, B. M. O'Brien, and E. P. Calius, J. Appl. Phys. **112**, 041101 (2012).
[25]S. Bauer, S. Bauer-Gogonea, I. Graz, M. Kaltenbrunner, C. Keplinger, and R. Schwödiauer, Adv. Mater. **26**, 149 (2014).
[26]P. Lochmatter and G. Kovacs, Sens. Actuators, A **141**, 577 (2008).
[27]A. Wingert, M. D. Lichter, and S. Dubowsky, IEEE/ASME Trans. Mechatronics **11**, 448 (2006).
[28]P. Chouinard and J. Plante, IEEE/ASME Trans. Mechatronics **17**, 857 (2012).
[29]J. S. Huang, T. Q. Lu, J. Zhu, D. R. Clarke, and Z. G. Suo, Appl. Phys. Lett. **100**, 211901 (2012).
[30]K. B. Subramani, E. Cakmak, R. J. Spontak, and T. K. Ghosh, Adv. Mater. **26**, 2949 (2014).
[31]Y. Wang, B. H. Chen, Y. Y. Bai, H. Wang, and J. X. Zhou, Appl. Phys. Lett. **104**, 064101 (2014).
[32]X. H. Zhao, W. Hong, and Z. G. Suo, Phys. Rev. B **76**, 134113 (2007).
[33]C. C. Foo, S. Q. Cai, S. J. A. Koh, S. Bauer, and Z. G. Suo, J. Appl. Phys. **111**, 034102 (2012).
[34]B. M. O'Brien, T. G. McKay, T. A. Gisby, and I. A. Anderson, Appl. Phys. Lett. **100**, 074108 (2012).